RESEARCH ARTICLE | AUGUST 15 2024

Role of strain softening and viscoelastic memory for the rolling friction of two tire tread compounds

Special Collection: JCP and CPR Editors' Choice 2024

N. Miyashita ; B. N. J. Persson

J. Chem. Phys. 161, 074702 (2024)
https://doi.org/10.1063/5.0223550

The Journal of Chemical Physics ARTICLE pubs.aip.org/aip/jcp

Role of strain softening and viscoelastic memory for the rolling friction of two tire tread compounds

Cite as: J. Chem. Phys. 161, 074702 (2024); doi: 10.1063/5.0223550
Submitted: 15 June 2024 • Accepted: 30 July 2024 •
Published Online: 15 August 2024

N. Miyashita[1] and B. N. J. Persson[2,3,4,a)]

AFFILIATIONS

[1] The Yokohama Rubber Company, 2-1 Oiwake, Hiratsuka, Kanagawa 254-8601, Japan
[2] State Key Laboratory of Solid Lubrication, Lanzhou Institute of Chemical Physics, Chinese Academy of Sciences, 730000 Lanzhou, China
[3] Peter Grünberg Institute (PGI-1), Forschungszentrum Jülich, 52425 Jülich, Germany
[4] MultiscaleConsulting, Wolfshovener Str. 2, 52428 Jülich, Germany

[a)] **Author to whom correspondence should be addressed:** b.persson@fz-juelich.de

ABSTRACT

Rolling friction is of great importance for many applications, such as tires and conveyor belts. We study the rolling friction for hard cylinders rolling on flat rubber sheets. The rolling friction depends on the number of rolling cycles, the rolling speed, and the temperature. We show that when the rubber is cooled down below the glass transition temperature, the deformations of the rubber surface are frozen-in, resulting in a non-flat rolling track where uphill and downhill rolling movements strongly affect the rolling force. The experimental data are analyzed using the Persson rolling friction theory; good agreement with the experiments is obtained when the non-linear (strain-softening) properties of the viscoelastic modulus are taken into account.

I. INTRODUCTION

Rubber rolling friction has many practical applications, e.g., in tires[1] and conveyor belts.[2] Here, we study the dependency of rolling friction on temperature, rolling speed, and the number of rolling cycles. We study how the rolling friction depends on time during repeated rolling over the same surface area. We find that in each rolling cycle, the rolling friction force differs from the previous rolling cycle. This is due to deformations of the rubber, which may require considerable time to disappear due to the wide distribution of rubber mechanical relaxation times. The same effect is the origin of the dependency of the force–displacement relation on time in oscillatory stress–strain studies using the Dynamic Mechanical Apparatus (DMA). It is also a well-known effect for cars: if a car is parked for a long time, the tires deform viscoelastically and a periodic noise is observed for some time during driving. In general, if a rubber block is exposed to a static force (or static deformation) for the time period t_0, (thermally activated) molecular rearrangement processes with relaxation times up to t_0 will be activated, and when the applied force is removed, a time period of order t_0 may be needed for the deformation field to fully disappear. This explains why a large time period may be needed before the tires become circular again after a long parking time period. (Note, however, that during rolling, the tire temperature increases, which shortens the recovery time.) This viscoelastic relaxation (or memory) effect could also explain some of the differences we observed between theory and experiments in our previous rolling friction study.[3]

In this study, we use two different styrene-butadiene (SB) compounds with a silica filler (compound A) and a carbon black filler (compound B). In the Appendix, we give the detailed composition of the two compounds, and Table I shows the glass transition temperatures T_g and the maximum of $\tan\delta$, as obtained from DMA measurements (see below).

TABLE I. Summary of the glass transition temperatures of compounds A and B. The glass transition temperature is defined as the maximum of $\tan\delta$ as a function of temperature at frequency $\omega_0 = 0.01\ \mathrm{s}^{-1}$.

Compound	T_g (°C)	Maximum of $\tan\delta$
A (33.8 wt. % silica)	−19.8	0.71
B (35.5 wt. % carbon)	−22.1	0.68

II. VISCOELASTIC MODULUS

We have measured the viscoelastic modulus for the rubber compounds A and B in elongation mode for the strain amplitude 4×10^{-4} (or 0.04% strain).[7] At this small strain, we probe the linear response properties of the rubber. We have performed measurements at different frequencies and different temperatures and shifted the frequency segments for $\mathrm{Re}E(\omega, T)$ to form a smooth master curve $\mathrm{Re}E(\omega, T) = \mathrm{Re}E(a_T\omega, T_{\mathrm{ref}})$, where the shift factor $a_T = 1$ at the reference temperature T_{ref}. The same shift factor a_T was used to obtain the master curve for $\mathrm{Im}E(\omega, T)$ (see Ref. 7 for more details).

In what follows, we denote $E(\omega, T)$ with $E(\omega)$ for simplicity. The accuracy of the measured modulus was tested by showing that the Kramers–Kronig relation, which relates $\mathrm{Re}E(\omega)$ to $\mathrm{Im}E(\omega)$, is satisfied. Figure 1(a) shows the real part ReE, and Fig. 1(b) shows the ratio $\mathrm{Im}E/\mathrm{Re}E = \tan\delta$ of the viscoelastic modulus for compounds A and B as a function of frequency.

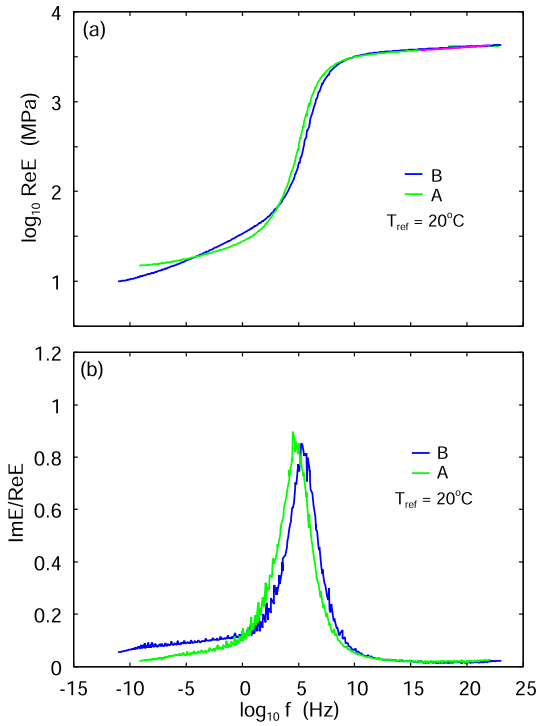

FIG. 1. (a) Real part ReE of the viscoelastic modulus for compounds A and B as a function of frequency (log–log scale). (b) The loss-tangent $\tan\delta$ as a function of the logarithm of the frequency. The reference temperature $T_{\mathrm{ref}} = 20\,^{\circ}\mathrm{C}$, and the strain $\epsilon = 0.0004$.

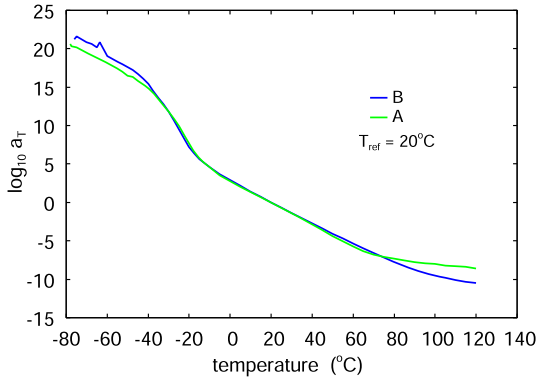

FIG. 2. Logarithm of the shift factor a_T as a function of temperature for compounds A and B at the reference temperature $T_{\mathrm{ref}} = 20\,^{\circ}\mathrm{C}$.

Figure 2 shows the temperature dependency of the logarithm of the shift factor a_T obtained when constructing the master curves for compounds A and B. The reference temperature $T_{\mathrm{ref}} = 20\,^{\circ}\mathrm{C}$, so $a_T = 1$ when $T = 20\,^{\circ}\mathrm{C}$.

Figure 3 shows for compound A the ratio $\tan\delta = \mathrm{Im}E(T, \omega)/\mathrm{Re}E(T, \omega)$ as a function of temperature T at the frequency $\omega_0 = 0.1\ \mathrm{s}^{-1}$. We have found that using the angular frequency $\omega_0 = 0.01\ \mathrm{s}^{-1}$, the temperature where $\tan\delta$ is maximal is nearly the same as the rubber glass transition temperature obtained using standard (viscosity or calorimetry) thermodynamic methods. For compound A $\tan\delta$ is maximal at $T \approx -19.8\,^{\circ}\mathrm{C}$, which we define as the glass transition temperature. Table I shows the glass transition temperatures and the maximum of $\tan\delta$ for compounds A and B.

Rubber rolling (or sliding) friction in most cases involves relatively large strain and depends on the non-linear viscoelastic properties of the rubber.[4–6] We have studied the large strain dependency of the effective modulus. The measurements were performed at the frequency $f = 1$ Hz in elongation mode at several different temperatures. Figure 4 shows the ratio $\eta_{\mathrm{R}}(\epsilon) = \mathrm{Re}E(\epsilon)/\mathrm{Re}E(0)$ (lower

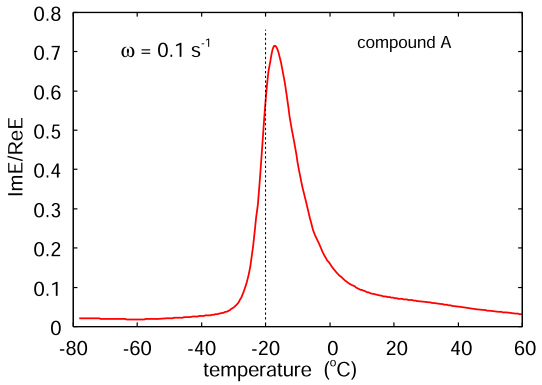

FIG. 3. Ratio $\mathrm{Im}E(T, \omega)/\mathrm{Re}E(T, \omega)$ as a function of temperature T at the frequency $\omega = 0.1\ \mathrm{s}^{-1}$ for compound A.

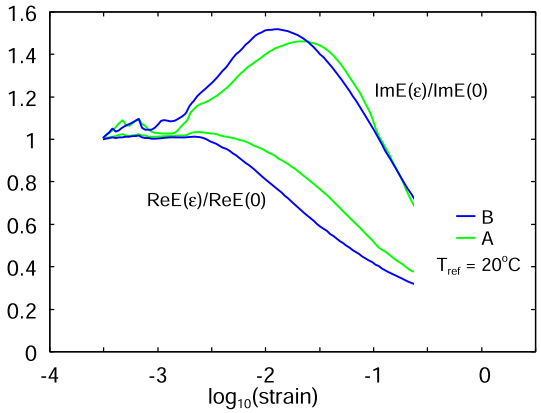

FIG. 4. Ratios $\mathrm{Re}E(\epsilon)/\mathrm{Re}E(0)$ (lower curves) and $\mathrm{Im}E(\epsilon)/\mathrm{Im}E(0)$ (upper curves) for the effective modulus at strain ϵ and at zero strain (actually, the strain ≈0.0001) as a function of strain ϵ. The results are the averages of the strain curves (for compounds A and B) obtained at temperatures $T = -10$, 0, 20, 60, and 100 °C.

curves) and $\eta_{\mathrm{I}}(\epsilon) = \mathrm{Im}E(\epsilon)/\mathrm{Im}E(0)$ (upper curves) for the effective modulus at strain ϵ and at zero strain (actually, the strain ≈0.0001) as a function of strain ϵ. The results are the averages of the strain curves obtained at temperatures $T = -10$, 0, 20, 60, and 100 °C. We have also performed strain sweeps in the shear mode, which gives qualitatively similar results as in the elongation mode. In Fig. 7, we show theory results using the non-linear modulus obtained in shear mode (blue curve) and in elongation mode (green curve).

III. ROLLING FRICTION THEORY FOR CYLINDERS

Here, we give the basic equations used to analyze the experimental results. The theory developed in Ref. 8 gives the rolling friction coefficient as a function of rolling speed for a rigid cylinder (radius R) rolling on a semi-infinite linear viscoelastic half-space. The theory in Ref. 8 is accurate and agrees very well with the exact result obtained for the simple rheology model used by Hunter.[9] In Ref. 10, the theory was found to be in good agreement with exact numerical simulations for a realistic viscoelastic modulus. In the present case, we assume that the cylinder is squeezed against a flat rubber sheet (thickness d) with the normal force per unit length $f_{\mathrm{N}} = F_{\mathrm{N}}/L$ and rolling at the speed v. If the width $2a$ of the cylinder–rubber contact region (in the rolling direction) $2a < d$, we can treat the rubber slab as infinitely thick. In this case, the rolling friction force, $F_{\mathrm{R}} = \mu_{\mathrm{R}} F_{\mathrm{N}}$, where the rolling friction coefficient[8]

$$\mu_{\mathrm{R}} \approx \frac{8 f_{\mathrm{N}}}{\pi} \int_0^\infty dq\ \mathrm{Im}\frac{1}{E_{\mathrm{eff}}(qv)} \frac{J_1^2(qa)}{(qa)^2}, \tag{1}$$

where $J_1(x)$ is the first order Bessel function and $E_{\mathrm{eff}}(\omega)$ is the effective viscoelastic modulus. The integration variable q can be considered as a wavenumber. The contact width $2a$ is given by the Hertz equation for cylinder contact,

$$a \approx \left(\frac{4 f_{\mathrm{N}} R}{\pi |E_{\mathrm{eff}}(qv)|}\right)^{1/2}. \tag{2}$$

In this equation, when used in (1), we take $|E_{\mathrm{eff}}| = |E_{\mathrm{eff}}(\omega)|$ with $\omega = qv$, so the contact width $2a$ depends on the rolling speed v.

The penetration $\delta = a^2/R$. The strain in the region where the viscoelastic deformations of the rubber occur varies in space but is typically of the order

$$\epsilon \approx \frac{\delta}{2a} \approx \frac{a}{2R} \approx \left(\frac{f_{\mathrm{N}}}{\pi |E_{\mathrm{eff}}(qv)| R}\right)^{1/2}. \tag{3}$$

As the rolling speed increases (or the temperature decreases), the effective modulus $E_{\mathrm{eff}}(qv)$ increases and the half-width a and the strain ϵ decrease. In the present case, at low rolling speeds, we find $\epsilon \approx 0.1$. In the study below, we will show theory results including strain softening. This has been obtained using the effective modulus $\mathrm{Re}E_{\mathrm{eff}}(\omega, \epsilon) = \mathrm{Re}E(\omega)\eta_{\mathrm{R}}(\epsilon)$ and $\mathrm{Im}E_{\mathrm{eff}}(\omega, \epsilon) = \mathrm{Im}E(\omega)\eta_{\mathrm{I}}(\epsilon)$ at the strain ϵ given by (3). This approach is, of course, only approximate since we use a theory based on linear viscoelasticity and only "correct" for the non-linearity using an effective modulus that depends on the average strain in the contact region, while the real strain varies in space. Still, the comparison to the experimental data (see below) shows that this approach gives a good estimate of the influence of strain softening on the rolling friction.

At the strain $\epsilon \approx 0.1$, from Fig. 4, we get $\eta_{\mathrm{R}} \approx 0.5$ and $\eta_{\mathrm{I}} \approx 1$. Since the rolling friction depends on $\mathrm{Im}E_{\mathrm{eff}}/|E_{\mathrm{eff}}|^2$, the non-linear correction will be $\approx \eta_{\mathrm{I}}/(\eta_{\mathrm{R}})^2 \approx 4$. That is, we expect the non-linear (strain softening) effects to enhance the rolling friction by roughly a factor of 4, in good agreement with the results presented below (see Figs. 7 and 16). When the rolling speed increases or the temperature decreases, the magnitude of the viscoelastic modulus, $|E_{\mathrm{eff}}(qv)|$, increases, and the strain, as given by (3), decreases. In the theory calculations, this is taken into account by using the measured $\eta_{\mathrm{R}}(\epsilon)$ and $\eta_{\mathrm{I}}(\epsilon)$ curves.

IV. ROLLING FRICTION

We have studied the rolling friction of compounds A and B using the same setup as in an earlier study (Ref. 3). In order to measure the rolling friction coefficient also at low temperatures, an experimental setup (a low-temperature linear friction slider) where the temperature can be changed from room temperature down to −40 °C should be used; see Fig. 5. The rollers are confined between two rubber sheets glued to steel plates, and one steel plate is attached to the force cell (the red block in the figure). The upper steel plate can move with the carriage in the vertical direction. The normal load can be changed by adding additional steel plates on top of the force cell. The substrate sample gets attached to the machine table, which is moved using a servo drive via a gearbox in a translational manner. Here, we control the relative velocity between the two rubber specimens and the substrate sample, while the force cell acquires information about normal force and the rolling friction force. To change the temperature, the whole setup is placed inside a deep freezer capable of cooling down to −40 °C.

Rubber sheets of compounds A and B were molded in the form of 1 cm thick sheets and glued to two flat steel plates (15 × 10 cm^2). We used polymethyl methacrylate (PMMA) cylindrical rollers with 1 cm diameter. The two cylinders were put between the rubber sheets, and a normal load was applied by adding steel plates on

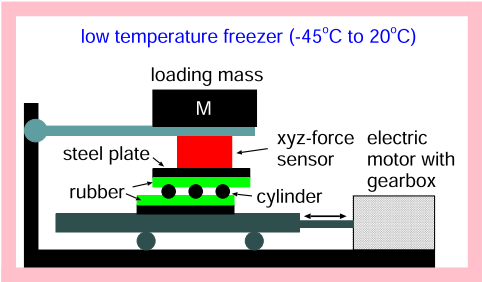

FIG. 5. Schematic picture of low-temperature friction instrument allowing for linear reciprocal motion. Several cylinders (say n) are rolling in between rubber sheets glued on steel blocks. The rubber sheets are 1 cm thick, and the PMMA cylinders are 1 cm in diameter. The steel blocks are squeezed with a normal force F_N, and the bottom plate moves with a velocity ranging from 10 μm/s to 1 cm s^{-1}.

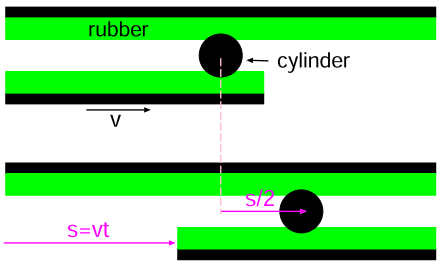

FIG. 6. A rigid cylinder squeezed between two rubber slabs glued to flat steel surfaces. The lower plate moves with the velocity v, and the roller exerts a force F on the upper plate. The rolling friction force $F = F_R$, and the rolling velocity $v_R = v/2$.

top of the upper rubber sheet. Figure 5 shows the experimental setup.

Figure 6 shows a rigid cylinder squeezed between two rubber slabs glued to flat steel surfaces. When the lower steel surface has moved a distance $s = vt$ relative to the upper steel surface, the rubber cylinder has rolled the distance $s/2$ relative to both steel surfaces. (This is most easily understood in a reference frame where the upper steel surface moves with velocity $v_x = v/2$ and the lower steel surface moves with $v_x = -v/2$; in this reference frame, by symmetry, the position of the cylinder does not change.) Hence, the rolling speed relative to both rubber slabs is $v/2$, and the force F needed to move the upper steel surface is given by the energy conservation condition $Fs = 2F_R \times (s/2)$, where F_R is the rolling force when the cylinder is rolling on one of the rubber slabs and the pre-factor 2 comes from the fact the cylinder is rolling on two rubber surfaces. Thus, we get $F = F_R$ and the rolling velocity $v_R = v/2$.

A. Rolling friction for compound A

Figure 7 shows the rolling friction master curve for compound A. The squares are the measured rolling friction values at the indicated temperatures shifted using the bulk viscoelastic shift factor a_T. The solid and dashed green lines are the calculated rolling friction coefficient with and without including strain softening. The blue line

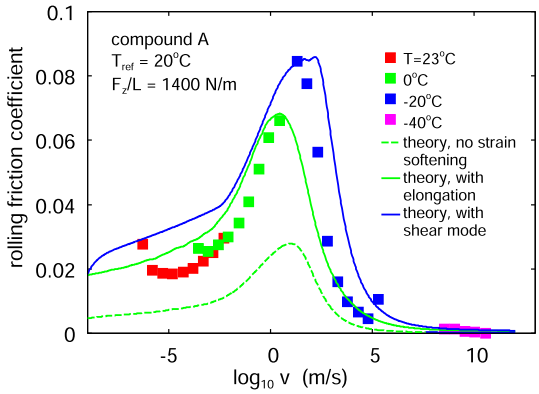

FIG. 7. Rolling friction master curve for compound A. The two Plexiglas cylinder rollers (each with 10 cm in contact with the rubber) have a diameter of 1 cm. The squares are the measured rolling friction values at the indicated temperatures shifted using the bulk viscoelastic shift factor a_T. The solid and dashed green lines are the calculated rolling friction coefficient with and without including the strain softening (in elongation). The blue line is the result where the strain softening was obtained in shear mode rather than in elongation mode as for the solid green line.

is the result where the strain softening was obtained in shear mode rather than in elongation mode as for the solid green line. The difference between the measured data (square symbols) and the theory (solid green and blue lines) is likely due to (a) inaccuracy in the strain softening measurement (see Fig. 4), (b) the simple way we take into account strain softening in the theory, and (c) the use of a rolling friction theory based on linear viscoelasticity for a problem involving non-linear viscoelasticity.

It is interesting to note the big influence of strain softening on the magnitude of the rolling friction.

We have also studied the dependency of the rolling friction on the number of rolling cycles. Figure 8 shows the tangential force F_x, divided by the normal force F_N, as a function of time for compound A at room temperature at (a) the start of the rolling friction experiments and (b) the end of the rolling friction experiments (after performing measurements at $T = 0$, -20, and $-40\,^\circ$C). Note that the temperature $T = 23\,^\circ$C in (a) and $T = 20\,^\circ$C in (b), which is, at least in part, the reason why the rolling friction force is slightly larger in (b).

In an ideal case, one would expect the rolling friction force to be time-independent when rolling in one direction, as shown by the black line in Fig. 9. However, the actual rolling friction force [blue line in the same figure, from the first rolling cycle in Fig. 8(a)] is not constant but depends on the position in the rolling contact. Note the dip (negative bump) in the measured force, which is in the same force direction (here toward a more negative force) when the rolling direction is reversed. Hence, the dip is not a rolling friction effect, since the rolling friction force changes sign when the rolling direction changes but must have a geometrical origin (see Fig. 10).

Figure 10 shows two geometrical effects, which may be the origin of the time (or x) dependency of the tangential force F_x in Fig. 9. In (a), an inhomogeneity in the rubber film thickness results in a tangential (non-friction) force when the roller moves uphill or downhill

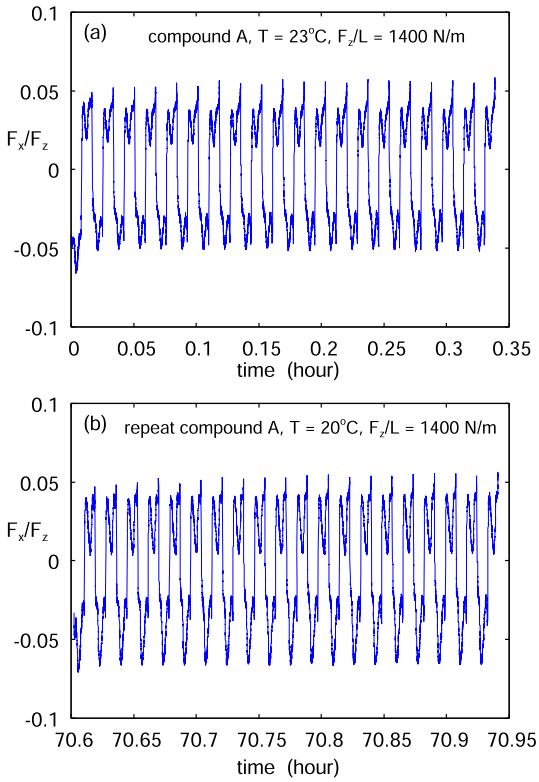

FIG. 8. Rolling force F_x divided by the normal force F_N as a function of time for compound A at room temperature at (a) the start of the rolling friction experiments and (b) the end of the rolling friction experiments (after performing measurements at $T = 0$, -20, and $-40\,^{\circ}\mathrm{C}$). Note that the temperature $T = 23\,^{\circ}\mathrm{C}$ in (a) and $T = 20\,^{\circ}\mathrm{C}$ in (b), which explains why the amplitude of the force fluctuations is slightly larger in (b). The rolling speed is $v = 1$ mm s^{-1}.

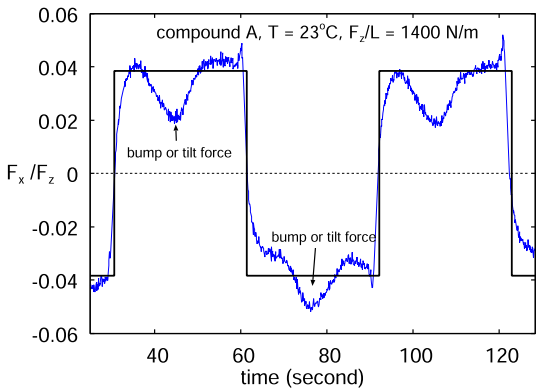

FIG. 9. Blue line: the rolling force F_x divided by the normal force F_N as a function of time for compound A at $T = 23\,^{\circ}\mathrm{C}$ [two cycles from Fig. 8(a)]. Black line: the ideal rolling friction force. Note the bump in the measured force, which is in the same force direction when the rolling direction is reversed. Hence, it is not due to rolling friction but must have a geometrical origin (see Fig. 10).

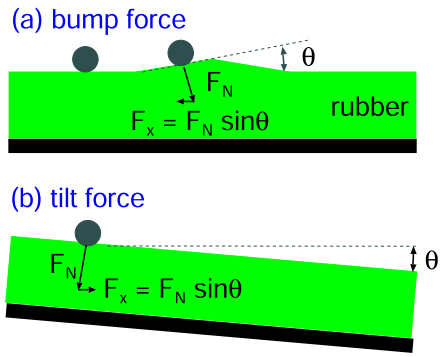

FIG. 10. (a) An inhomogeneity in the rubber film thickness, or in the glue film thickness between the rubber sheet and the steel plate below, will result in a tangential force when the roller moves past the bump. This force is caused by the non-flatness of the rubber surface, and we denote it as a bump force. (b) Similarly, a tilting of the rubber sheet will give rise to a tangential force, which has the same direction independent of the rolling direction in contrast to the friction force, which changes sign when the rolling direction changes. To obtain the true rolling friction force (caused by energy dissipation), we average the measured tangential force over the forward rolling direction and over the backward rolling direction, subtracting the two and dividing by two to obtain the rolling friction force.

on the bump. This force is caused by the non-flatness of the rubber surface, which results in an uphill and downhill force on the slider; we denote this as a *bump-force*. Similarly, a slight tilting (which is unavoidable) of the rubber sheet as in (b) will give rise to a tangential force that has the same lateral direction independent of the rolling direction in contrast to the friction force that changes sign when the rolling direction changes. We denote this force as a *tilt-force*. To obtain the rolling friction force (caused by energy dissipation), we average the measured tangential force over the forward rolling direction, and over the backward rolling direction, subtracting the two and dividing by two to obtain the rolling friction force. We note that *averaging over forward and backward sliding motions* removes the contribution from the tilt and bump forces.

Figures 11 and 12 shows similar results as in Fig. 8 at $T = 0$ and $-20\,^{\circ}\mathrm{C}$, respectively. Note that while the tangential force does not

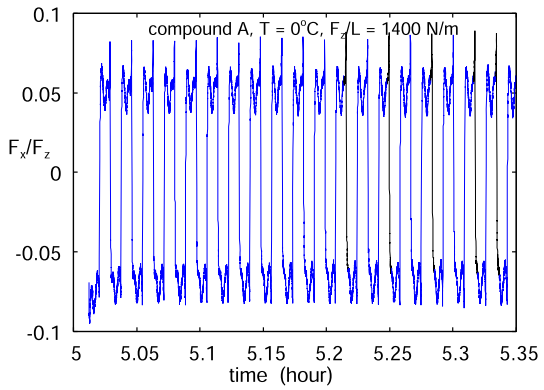

FIG. 11. Rolling force F_x divided by the normal force F_N as a function of time for compound A at $T = 0\,^{\circ}\mathrm{C}$.

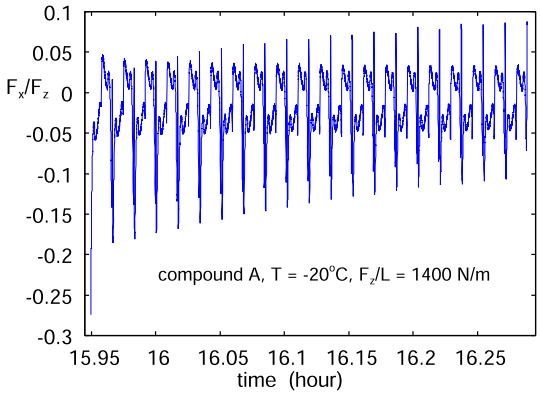

FIG. 12. Rolling force F_x divided by the normal force F_N as a function of time for compound A at $T = -20\,^{\circ}\mathrm{C}$.

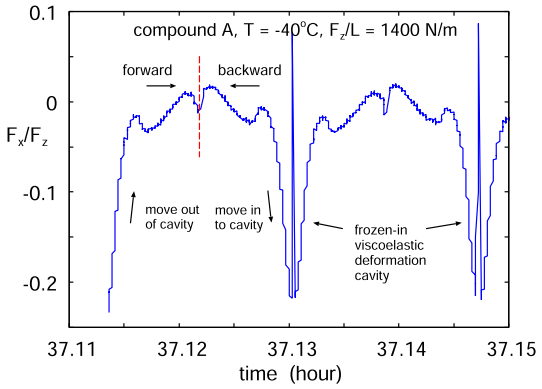

FIG. 14. Rolling force F_x divided by the normal force F_N as a function of time for compound A at $T = -40\,^{\circ}\mathrm{C}$ on a short time interval involving two rolling cycles.

change with increasing number of cycles when $T = 20\,^{\circ}\mathrm{C}$ (or 0 or $-40\,^{\circ}\mathrm{C}$), at $T = -20\,^{\circ}\mathrm{C}$, the magnitude of the minimum tangential force F_x decreases with increasing number of cycles. The minimum force is due to the following viscoelastic bump (or rather cavity) effect: the cooling of the system from $T = 0\,^{\circ}\mathrm{C}$ to $T = -20\,^{\circ}\mathrm{C}$ takes a long time (about 10 h). During this time, a roller is stationary, say located at $x = 0$, and squeezed against the rubber sheets. At $T = 0\,^{\circ}\mathrm{C}$, on the time scale of the static contact (10 h), the rubber is in the rubbery region and the roller will produce a large (elastic deformation) indentation in the rubber. When the system is cooled down to $T = -20\,^{\circ}\mathrm{C}$, the rubber relaxation times become relatively long, so when the rolling starts, it will roll uphill to come out of the indentation cavity, which will result in a (non-friction) contribution to the tangential force. During the following 20 rolling cycles, the indentation cavity decreases in height due to viscoelastic relaxation. This is the reason why the magnitude of the minimum tangential force, which is due to moving out of the indentation well at $x = 0$, is decreasing with increasing rolling time (Fig. 13). At $T = 0\,^{\circ}\mathrm{C}$, the system is in the rubbery region on the time scale of one rolling cycle (about 60 s), and the indentation will disappear already during the first rolling cycle.

At $T = -40\,^{\circ}\mathrm{C}$, the rubber is in the glassy region (see Fig. 3) and the indentation well is frozen-in (see Fig. 13) and the magnitude of the minimum tangential force does not depend on the number of rolling cycles. For this case, Fig. 14 shows the rolling friction force F_x divided by the normal force F_N as a function of time during the first two rolling cycles. Note that the tangential force is nearly the same during forward and backward rolling motion, which implies that *nearly the whole tangential force is a geometrical effect* resulting from the (frozen-in) deformed rubber surface. That is, the whole structure shown in Fig. 14 is due to the frozen-in elastic deformations from the earlier time period where the PMMA cylinders were stationary during the cooling from above to below the glass transition temperature. This frozen-in deformations give a tangential force in the same direction independent rolling direction. This explains why the tangential force is symmetric around the turn-around position

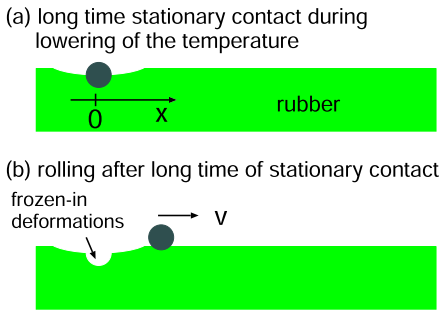

FIG. 13. During lowering of the temperature, the roller is in stationary contact (say at $x = 0$). When the temperature is lowered below the glass transition temperature (about $-20\,^{\circ}\mathrm{C}$ for compound A), the elastic deformations are frozen-in and remain during the following rolling cycles and will result in a tangential force every time the roller returns to the initial position $x = 0$.

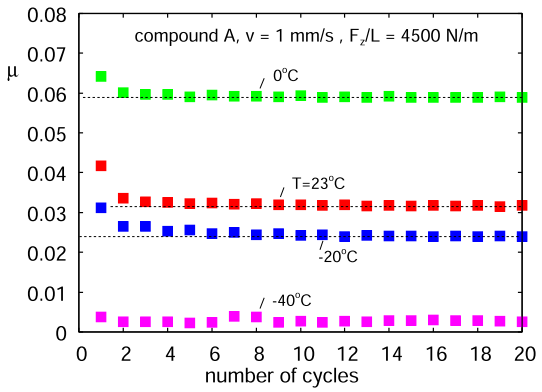

FIG. 15. Rolling friction coefficient μ as a function of the number of rolling cycles. The rolling friction force (caused by energy dissipation) is obtained for each rolling cycle by averaging the measured tangential force over the forward rolling direction and over the backward rolling direction, subtracting the two and dividing by two.

rather than antisymmetric as would be the case for a true friction force. Thus, at $T = -40\,^{\circ}\mathrm{C}$, the rolling friction force nearly vanishes (see Fig. 15), as indeed expected when the rubber is in the glassy region, where the response is elastic rather than viscoelastic.

Removing the geometrical (bump or tilt) contribution to the tangential force results, at all temperatures, in a rolling friction force, which is nearly independent of the number of rolling cycles. This is illustrated in Fig. 15, which shows the rolling friction coefficient μ as a function of the number of rolling cycles. The rolling friction force (caused by energy dissipation) is obtained for each rolling cycle by averaging the measured tangential force over the forward rolling direction, and over the backward rolling direction, subtracting the two and dividing by two. The rolling friction force is nearly constant beyond the second rolling cycle but drops by a non-negligible amount between the first and second rolling cycles.

B. Rolling friction for compound B

Figure 16 shows the rolling friction master curve for compound B. The squares are the measured rolling friction values at the indicated temperatures shifted using the bulk viscoelastic shift factor a_T. The solid and dashed green lines are the calculated rolling friction coefficient with and without including strain softening. The difference between the measured data (square symbols) and the theory (solid green line) is likely mainly due to inaccuracy in the strain softening measurement (see Fig. 4) and the simple way we take into account strain softening in the theory.

It is interesting to note the big influence of strain softening on the magnitude of the rolling friction.

We have also studied the dependency of the rolling friction on the number of rolling cycles. Figure 17 shows the tangential friction force F_x, divided by the normal force F_N, as a function of time for compound B at room temperature at the start of the rolling friction experiments (red curve) and at the end of the rolling friction experiments (green curve) (after performing measurements between $T = 10$ and $-40\,^{\circ}\mathrm{C}$). Note that the temperature $T = 23\,^{\circ}\mathrm{C}$ in the first

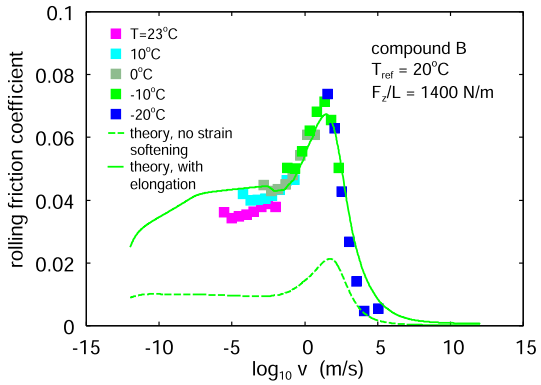

FIG. 16. Rolling friction master curve for compound B. The two Plexiglas cylinder rollers (each with 10 cm in contact with the rubber) have a diameter of 1 cm. The squares are the measured rolling friction values at the indicated temperatures shifted using the bulk viscoelastic shift factor a_T. The solid and dashed green lines are the calculated rolling friction coefficient with and without including strain softening.

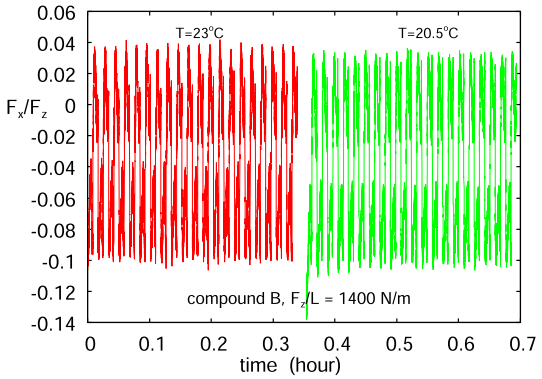

FIG. 17. Rolling force F_x divided by the normal force F_N as a function of time for compound B at $T = 20\,^{\circ}\mathrm{C}$.

experiment and $T = 20.5\,^{\circ}\mathrm{C}$ in the second (repeat) experiment. Note also that the force $F_x(t)$ extends to much more negative force values during the backward rolling motion than it extends toward positive force values during the forward rolling motion. This must be due to a tilting of the substrate rubber sample, i.e., it is not perfectly horizontal, resulting in a tangential tilt force, which shifts the force curve toward a more negative force.

Figure 18 shows the rolling friction force F_x divided by the normal force F_N as a function of time during the first two rolling cycles at $T = -40\,^{\circ}\mathrm{C}$. Note that the tangential force is nearly the same during forward and backward rolling motions, which implies that nearly the whole tangential force is a geometrical effect resulting from the deformed rubber surface. Thus, at $T = -40\,^{\circ}\mathrm{C}$, the rolling friction force nearly vanishes, as indeed expected when the rubber is in the glassy region where the response is elastic rather than viscoelastic.

Removing the geometrical (bump or tilt) contribution to the tangential force results, at all temperatures, in a rolling friction force, which is nearly independent of the number of rolling cycles. This is illustrated in Fig. 19, which shows the rolling friction coefficient μ as a function of the number of rolling cycles. The rolling friction force (caused by energy dissipation) is obtained for each rolling cycle

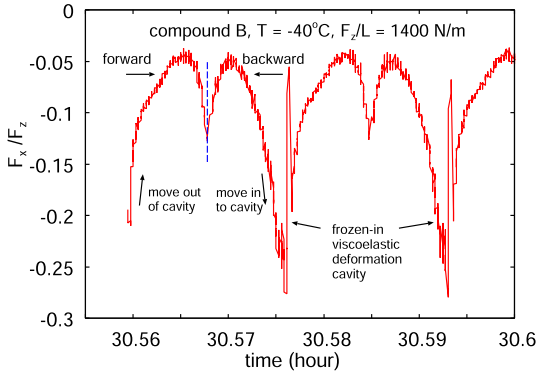

FIG. 18. Rolling force F_x divided by the normal force F_N as a function of time for compound B at $T = -40\,^{\circ}\mathrm{C}$.

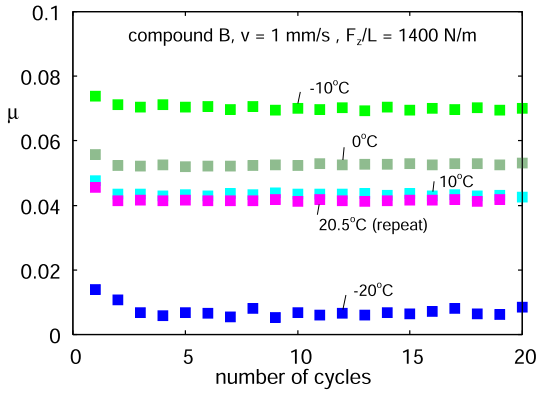

FIG. 19. Rolling friction coefficient μ as a function of the number of rolling cycles. The rolling friction force (caused by energy dissipation) is obtained for each rolling cycle by averaging the measured tangential force over the forward rolling direction and over the backward rolling direction, subtracting the two and dividing by two.

by averaging the measured tangential force over the forward rolling direction, and over the backward rolling direction, subtracting the two and dividing by two. The rolling friction force is nearly constant beyond the second rolling cycle but drops by a non-negligible amount between the first and second rolling cycles.

V. SUMMARY AND OUTLOOK

We have studied how rolling friction depends on time during repeated rolling over the same surface area. We find that in each rolling cycle, the rolling friction force will differ from the previous rolling cycle, in particular when the temperature is close to the rubber glass transition temperature. This is due to deformations of the rubber that may require considerable time to disappear due to the wide distribution of rubber mechanical relaxation times. This effect is particularly strong when the system (with the rollers squeezed against the rubber) is cooled below the rubber glass transition temperature. This results in frozen-in deformations of the rubber surface, which result in uphill and downhill movements of the rollers as they move out or into the deformed regions. In general, we find good agreement between the measured friction data and the theory but only when the non-linear properties of the viscoelastic modulus are taken into account. We account for the non-linear effects in the simplest possible way by scaling the linear response modulus with strain-dependent factors obtained from DMA strain sweep data.

The tilt and bump effects described above will affect the tangential force in all rolling or sliding friction studies using linear friction sliders. To eliminate its influence on the measured friction coefficient, one should always average the friction force over one cycle of forward and backward rolling (or sliding) motions. We have observed tilt and bump effects before, e.g., in sliding on ice, where additional problems occur related to ice wear processes as the slider hits into ice bumps.[11]

In the study presented above, adhesion has a negligible influence on friction. At a much smaller normal force than used here, and for very smooth surfaces, adhesion will be important.[12–14] The adhesive contribution to rolling friction is determined by energy dissipation at the opening crack and energy gain at the closing crack, but the latter can often be neglected. If the energy dissipation in the bulk due to the process studied in this paper can be neglected, the rolling friction is determined by the theory of cracks in viscoelastic solids.[15–18] We plan to study this in another publication using the same experimental setup as used in this study but with a smaller normal force[19] and more rollers.

AUTHOR DECLARATIONS

Conflict of Interest

The authors have no conflicts to disclose.

Author Contributions

N. Miyashita: Conceptualization (equal); Data curation (equal); Formal analysis (equal); Writing – original draft (equal); Writing – review & editing (equal). **B. N. J. Persson**: Conceptualization (equal); Data curation (equal); Formal analysis (equal); Investigation (equal); Writing – original draft (equal); Writing – review & editing (equal).

DATA AVAILABILITY

The data that support the findings of this study are available from the corresponding author upon reasonable request.

APPENDIX: RUBBER COMPOSITION

In Table II, we show the composition of the rubber compounds A and B. The cure condition for compound A was 40 min. at 160 °C and, for compound B, 15 min at 160 °C. The rubber was prepared in thin sheets, 1 and 10 mm thick, where the former was used for the DMA measurements and the latter was used for the rolling friction studies. Note that with respect to rolling friction, a rubber sheet can be treated as infinitely thick if the width of the cylinder–rubber contact region (in the rolling direction) is much smaller than the thickness of the rubber sheet.

TABLE II. Composition of the rubber compounds A and B.

Mass wt. %	Compound A	Compound B
SBR	56.2	59.2
Silica	33.8	0
Silane coupling agent	2.7	0
Vulcanization activator	1.7	0
Carbon black	0	35.5
Zinc oxide	1.7	1.8
Stearic acid	1.1	1.8
Antioxidant	<1	<1
Vulcanization accelerator (I)	<1	<1
Vulcanization accelerator (II)	<1	0
Sulfur	1.1	1.2

REFERENCES

[1] E. Riahi, M. T. Do, and M. Kane, "An energetic approach to model the relationship between tire rolling friction and road surface macrotexture," Surf. Topogr.: Metrol. Prop. **10**, 014001 (2022).

[2] B. N. J. Persson, "Conveyor belt drive physics," Tribol. Lett. **68**, 17 (2020).

[3] A. Tiwari, N. Miyashita, and B. N. J. Persson, "Rolling friction of elastomers: Role of strain softening," Soft matter **15**, 9233 (2019).

[4] *Modeling of Non-linear Viscoelastic Behavior of Filled Rubbers*, *Vol. 264 Advances in Polymer Science*, edited by D. Ponnamma and S. Thomas (Springer, 2014).

[5] G. Heinrich and M. Klüppel, in *Recent Advances in the Theory of Filler Networking in Elastomers*, *Vol. 160 Advances in Polymer Science*, edited by K.-S. Lee (Springer-Verlag, Berlin, Heidelberg, 2002), pp. 1–44.

[6] T. V. Tolpekina, W. Pyckhout-Hintzen, and B. N. J. Persson, "Linear and nonlinear viscoelastic modulus of rubber," Lubricants **7**, 22 (2019), see, e.g. and references therein.

[7] B. Lorenz, W. Pyckhout-Hintzen, and B. N. J. Persson, "Master curve of viscoelastic solid: Using causality to determine the optimal shifting procedure, and to test the accuracy of measured data," Polymer **55**, 565 (2014).

[8] B. N. J. Persson, "Rolling friction for hard cylinder and sphere on viscoelastic solid," Eur. Phys. J. E **33**, 327 (2010).

[9] S. C. Hunter, "The rolling contact of a rigid cylinder with a viscoelastic half space," J. Appl. Mech. **28**(4), 611 (1961).

[10] M. Scaraggi and B. N. J. Persson, "Rolling friction: Comparison of analytical theory with exact numerical results," Tribol. Lett. **55**, 15 (2014).

[11] N. Miyashita, A. E. Yakini, W. Pyckhout-Hintzen, and B. N. J. Persson, "Sliding friction on ice," J. Chem. Phys. **158**, 174702 (2023).

[12] G. Carbone, C. Mandriota, and N. Menga, "Theory of viscoelastic adhesion and friction," Extreme Mech. Lett. **56**, 101877 (2022).

[13] R. Nazari, A. Papangelo, and M. Ciavarella, "Friction in rolling a cylinder on or under a viscoelastic substrate with adhesion," Tribol. Lett. **72**, 50 (2024).

[14] A. Papangelo, R. Nazari, and M. Ciavarella, "Friction for a sliding adhesive viscoelastic cylinder: Effect of Maugis parameter," Eur. J. Mech., A: Solids **107**, 105348 (2024).

[15] C. Y. Hui, B. Zhu, and R. Long, "Steady state crack growth in viscoelastic solids: A comparative study," J. Mech. Phys. Solids **159**, 104748 (2022), see and references therein.

[16] B. N. J. Persson and E. A. Brener, "Crack propagation in viscoelastic solids," Phys. Rev. E **71**, 036123 (2005).

[17] B. N. J. Persson, "On opening crack propagation in viscoelastic solids," Tribol. Lett. **69**, 115 (2021).

[18] M. H. Müser and B. N. J. Persson, "Crack and pull-off dynamics of adhesive, viscoelastic solids," Europhys. Lett. **137**, 36004 (2022).

[19] The friction slider used in the present study has a minimum normal force of about 200 N. The instrument is now redesigned with a minimum normal force around 50 N.